

## **Pleiotropic effect of Lactoferrin in the prevention and treatment of COVID-19 infection: *in vivo*, *in silico* and *in vitro* preliminary evidences**

Campione Elena,<sup>1\*</sup> Lanna Caterina,<sup>1</sup> Cosio Terenzio,<sup>1</sup> Rosa Luigi,<sup>2</sup> Conte Maria Pia,<sup>2</sup> Iacovelli Federico,<sup>3</sup> Romeo Alice,<sup>3</sup> Falconi Mattia,<sup>3</sup> Del Vecchio Claudia,<sup>4</sup> Franchin Elisa,<sup>4</sup> Lia Stella,<sup>5</sup> Miniero Marilena,<sup>5</sup> Chiaramonte Carlo,<sup>6</sup> Ciotti Marco,<sup>7</sup> Nuccetelli Marzia,<sup>8</sup> Terrinoni Alessandro,<sup>5</sup> Ilaria Iannuzzi,<sup>9</sup> Coppeda Luca,<sup>9</sup> Magrini Andrea,<sup>9</sup> Moricca Nicola,<sup>10</sup> Sabatini Stefano,<sup>10</sup> Rosapepe Felice,<sup>11</sup> Bartoletti Pier Luigi,<sup>12</sup> Bernardini Sergio,<sup>8</sup> Andreoni Massimo,<sup>13</sup> Valenti Piera,<sup>2§</sup> Bianchi Luca<sup>1§</sup>

<sup>1</sup>Dermatology Unit, University of Rome “Tor Vergata”, Rome, 00133, Italy.

<sup>2</sup>Department of Public Health and Infectious Diseases, University of Rome “La Sapienza”, 00185, Italy.

<sup>3</sup>Department of Biology, Structural Bioinformatics Group, University of Rome “Tor Vergata”, Rome, 00133, Italy.

<sup>4</sup>Department of Molecular Medicine, University of Padova, 35122 Padova, Italy.

<sup>5</sup>Department of Experimental Medicine, Tor Vergata University Hospital, Rome, 00133, Italy.

<sup>6</sup>Departement of statistics, University of Rome Tor Vergata, Rome, 00133, Italy.

<sup>7</sup>Virology Unit, Tor Vergata University Hospital, Rome, 00133, Italy.

<sup>8</sup>Laboratory Medicine, Department of Experimental Medicine and Surgery, Tor Vergata University Hospital,

<sup>9</sup>Occupational Medicine Department, University of Rome "Tor Vergata", Rome, 00133, Italy.

<sup>10</sup>Villa dei Pini Hospital, Anzio (RM), Italy.

<sup>11</sup>Pineta Grande Hospital, Caserta, Italy

<sup>12</sup>Fimmg provincial, Rome, Italy

<sup>13</sup>Infectious Disease Unit, Tor Vergata University Hospital, Rome, 00133, Italy

<sup>§</sup>Those authors equally contributed as senior authors

**Correspondence:** elena.campione@uniroma2.it; campioneelena@hotmail.com

## SUMMARY

The current treatments against SARS-CoV-2 have proved so far inadequate. A potent antiviral drug is yet to be discovered. Lactoferrin, a multifunctional glycoprotein, secreted by exocrine glands and neutrophils, possesses an antiviral activity extendable to SARS-Cov-2.

We performed a randomized, prospective, interventional study assessing the role of oral and intranasal lactoferrin to treat mild-to-moderate and asymptomatic COVID-19 patients to prevent disease evolution. Lactoferrin induced an early viral clearance and a fast clinical symptoms recovery in addition to a statistically significant reduction of D-Dimer, Interleukin-6 and ferritin blood levels. The antiviral activity of lactoferrin related to its binding to SARS-CoV-2 and cells and *protein-protein docking methods*, provided the direct recognition between lactoferrin and spike S, thus hindering the spike S attachment to the human ACE2 receptor and consequently virus entering into the cells.

Lactoferrin can be used as a safe and efficacious natural agent to prevent and treat COVID-19 infection.

**KEYWORDS:** lactoferrin, COVID-19, SARS-CoV2

## INTRODUCTION

In December 2019, in Whuan, China, a cluster of pneumonia cases was observed. This cluster was related to a novel member of *Betacoronavirus*, named SARS-CoV-2, possessing more than 80% identity to SARS-CoV and 50% to the MERS-CoV (Lu et al., 2020; Tian et al., 2020). Coronavirus are spherical, enveloped viruses possessing a single-strand, positive-sense RNA genome ranging from 26 to 32 kilobases in length (Su et al., 2016). Their genome encodes 16 non-structural proteins (Menachery et al., 2014), accessory proteins (Forni et al., 2017) and 4 essential structural proteins, namely spike S glycoprotein, small envelope protein, matrix protein, and nucleocapsid protein (Lan et al., 2020). Homotrimeric S glycoprotein, possessing N-linked glycans, is located on the envelope and comprises two subunits (S1 and S2) in each spike monomer (Cui et al., 2019). As homotrimers of S glycoproteins are exposed on the viral surface, they are responsible for binding to host receptors (S1) and membrane fusion (S2) (Li, 2016; Lu et al., 2020). Cryo-electron microscopy on S protein has highlighted its interaction with cell receptor angiotensin-converting enzyme 2 (ACE2) and the dissociation of S1 after binding to the host cells. This leads S2 to a more stable state, pivotal for membrane fusion (Gui et al., 2017; Kirchdoerfer et al., 2018; Yuan et al., 2017). Apart from ACE2, also the heparan sulfate proteoglycans [HSPGs], localized on the cell surface, have been recognized as the binding sites for SARS-CoV (Lang et al., 2011) and could be important also for SARS-CoV-2 in the early attachment phase.

Lately, Wrapp and coworkers (Wrapp et al., 2020), determined the first 3.5 Å resolution cryo-electron microscopy [cryo-EM] structure of the SARS-CoV-2 S trimer in the prefusion conformation. Because of the critical function of spike S glycoprotein in the SARS-CoV-2 infection process, the knowledge

of this structure, which represents a target for antibody, protein and drug mediated neutralization, allowed to get atomic-level information able to guide the design and development of innovative therapeutic molecules(Romeo et al., 2020).

So far, the current treatment approaches have proved inadequate and a potent antiviral drug is yet to be discovered. Asymptomatic and mildly symptomatic patients remain a transmission reservoir, with possible evolution to the most severe disease form, without a clear treatment indication. Innate immunity should be better investigated to individuate a possible molecule with antiviral activity against COVID-19, especially considering the fact that children, where innate immunity is more prominent(Chang, R et al., 2020), are less likely to suffer of severe and critical COVID-19 disease than adults (Carsetti et al., 2020; Ludvigsson, 2020). Considering all these aspects, lactoferrin (Lf), a multifunctional glycoprotein, belonging to the transferrin family, secreted by exocrine glands and neutrophils and present in all human secretion(Rosa et al., 2017; Valenti and Antonini, 2005), represents the ideal candidate to fight SARS-CoV-2(Campione et al., 2020).

Indeed, two promising *in vitro* studies, the first on SARS-CoV (Lang et al., 2011) and the second on SARS-CoV-2 (Mirabelli et al., 2020) have demonstrated that Lf is able to inhibit the early phase of these two viruses and is efficient against SARS-CoV-2 also in post-infection phase(Mirabelli et al., 2020).

The pleiotropic activity of Lf is mainly based on its four different functions: to chelate two ferric iron per molecule, interact with anionic molecules, enter inside the nucleus and modulate iron homeostasis. The ability to chelate two ferric ions per molecule is associated to the inhibition of reactive oxygen species formation and the sequestration of iron, which is important for bacterial and viral replication and is at the basis of the antibacterial and antiviral activity of Lf (Berlutti et al., 2011; Valenti and Antonini, 2005; Wakabayashi et al., 2014). The binding to the anionic surface compounds, thanks to its cationic feature, is associated to the host protection against bacterial and viral adhesion and entry (Valenti and Antonini, 2005). The entrance inside host cells and the translocation into the nucleus (Ashida et al., 2004; Lepanto et al., 2019) is related to the anti-inflammatory activity of Lf (Kruzel et al., 2017; Liao et al., 2012; Suzuki et al., 2008) and its ability to modulate iron homeostasis perturbed by viral infection and inflammation (Mancinelli et al., 2020). As matter of fact, iron homeostasis involves several iron proteins such as transferrin, ferroportin, hepcidin and ferritin the disorders of which, induced by inflammation, lead to intracellular iron overload and viral replication (Campione et al., 2020). Moreover, Lf seems to regulate the activation of plasminogen and control coagulation cascade with a remarkable antithrombotic activity(Zwirzitz et al., 2018), a very frequent complication of SARS-CoV2 (Marietta et al., 2020). In addition to all these abilities, Lf, as above reported, inhibits the early phase of SARS-CoV (Lang et al., 2011) and

post-infection phase of SARS-CoV-2 (Lang et al., 2011; Mirabelli et al., 2020) probably through the binding to HSPGs or to viral particles.

Therefore, based on this information, in order to evaluate the possibility of using Lf in the clinical treatment of Covid-19, a clinical trial has been designed to validate the aforementioned assumptions together with *in vitro* experimental assays and simulation.

In particular, we designed a prospective, interventional study in order to assess the role of oral and intra-nasal liposomal lactoferrin for COVID-19 patients with mild-to-moderate disease and COVID-19 asymptomatic patients, and document its efficacy in improving symptoms and clearing away the virus. To study the mechanism of anti-viral activity of Lf against SARS-CoV-2, *in vitro* experimental assays have been designed to validate the abovementioned postulations. The hypothesis of the putative binding between spike and Lf and between viral units and host cells HSPGs has been verified *in vitro* thus preliminarily demonstrating Lf antiviral activity against SARS-CoV-2. Furthermore, the SARS-CoV-2 S trimer structure in prefusion conformation (Wrapp et al., 2020) has been used to perform a protein-protein molecular docking analysis with the aim to confirm the hypothesis of a direct interaction between the Spike S glycoprotein and the Lf protein. The structure of the spike glycoprotein (Wrapp et al., 2020) has been completed using modelling techniques and used to predict Lf interaction sites. Furthermore, the selected high-score protein-protein complex has been structurally investigated using classical molecular dynamics (MD) simulation and the free energy of interaction between these proteins has been evaluated through the molecular mechanic energies combined with generalized Born and surface area continuum solvation (MM/GBSA) method (Genheden and Ryde, 2015).

## **MATERIALS & METHODS**

### **Clinical trial**

We performed a randomized, prospective, interventional study to assess the efficacy of a liposomal formulation of apolactoferrin in COVID-19 patients with mild-to-moderate disease and COVID-19 asymptomatic patients. Mild-to-moderate disease was defined based on less severe clinical symptoms with no evidence of pneumonia and not requiring Intensive Care Unit (ICU) (Xu et al., 2020a)

The primary endpoint was real-time reverse transcription polymerase chain reaction (rRT-PCR) negative conversion rate of SARS-COV-2 RNA.

The secondary endpoints were the identification of COVID-19 deranged blood parameters and therefore treatment target markers and rate of disease remission, defined as symptoms recovery and blood parameters improvement. In addition, safety and tolerability of liposomal apolactoferrin for oral and intra-nasal use was assessed.

### *Patients (study population)*

Eligible patients were over 20 years old, with a confirmed COVID-19 rRT-PCR at the naso-oropharyngeal swab and blood oxygen saturation (SPO<sub>2</sub>) > 93% or Horowitz index (PaO<sub>2</sub> / FiO<sub>2</sub>) > 300mmHg. Patients did not receive any other treatment against SARS-CoV-2. Exclusion criteria included pregnancy and breastfeeding, nitric oxide and nitrates assumptions, known allergy to milk proteins, a medical history of bronchial hyperactivity or pre-existing respiratory diseases. ICU COVID in-patients were excluded.

A control group of healthy volunteers, with negative rRT-PCR at the naso-oropharyngeal swab, was included in the study in order to be paired to the above case-group. The "matched-pair-analysis" concerned the structural and clinical characteristics of the corresponding group. Placebo or liposome arms have not been included due to ethical reasons.

All patients gave written informed consent after receiving an extensive disclosure of the study purposes and risks. To be included, patients needed to be able to understand the content of informed consent and accept to sign it. The trial was approved by the Tor Vergata University Hospital Ethics Committee (Code 42/20). It was registered at [www.clinicalTrials.gov](http://www.clinicalTrials.gov) (NCT04475120) and reported according to CONSORT guidelines (Fig. S4, supplemental data).

### *Study design*

COVID-19 patients were consecutively enrolled from 22 April 2020 to 22 June 2020 from the University Hospital of Rome Tor Vergata, from Pineta Grande Hospital of Caserta and Villa dei Pini Hospital Anzio (Rome). The scheduled dose treatment of liposomal apolactoferrin for oral use was 1gr per day for 30 days (10 capsules per day) in addition to the same formulation intranasally administered 3 times daily.

Apolactoferrin capsules contain 100 mg of apo-Lf encapsulated in liposome while apolactoferrin nasal spray contains about 2.5 mg/ml of apo-Lf encapsulated in liposome. Apo-Lf, contained in both products, was checked by SDS-PAGE and silver nitrate staining and its purity was about 95%. The apo-Lf iron saturation was about 5% as detected by optical spectroscopy at 468 nm based on an extinction coefficient of 0.54 (100% iron saturation, 1% solution).

The control group of healthy volunteers did not receive any treatment or placebo.

### *Endpoints measures*

rRT-PCR was performed at T<sub>0</sub>, T<sub>1</sub>(after 15 days) and T<sub>2</sub> (after 30 days) to detect SARS-CoV-2 RNA in the study population.

All participants (COVID-19 patients and control group) underwent the following laboratory tests: complete blood count and chemistry panel (liver and kidney function), iron panel, coagulation profile, IL-6, IL-10, TNF $\alpha$ , adrenomedullin serum levels. COVID-19 patients' blood samples were collected at T0 and T2; control group's blood samples were collected at T0.

Body temperature and evaluation of related signs and symptoms were collected at T0, T1 and T2 in COVID-19 patients.

### ***In vitro antiviral activity of lactoferrin***

For *in vitro* experiments, highly purified bovine lactoferrin (bLf) was kindly provided by Armor Proteines Industries (France). BLf was checked by SDS-PAGE and silver nitrate staining. Its purity was about 98% and its concentration was confirmed by UV spectroscopy according to an extinction coefficient of 15.1 (280 nm, 1% solution). The bLf iron saturation was about 7% as detected by optical spectroscopy at 468 nm based on an extinction coefficient of 0.54 (100% iron saturation, 1% solution). LPS contamination of bLf, estimated by Limulus Amebocyte assay (Pyrochrome kit, PBI International, Italy), was equal to  $0.6 \pm 0.05$  ng/mg of bLf. Before each *in vitro* assays, bLf solution was sterilized by filtration using 0.2  $\mu$ m Millex HV at low protein retention (Millipore Corp., Bedford, MA, USA).

### ***Cell culture and virus***

The African green monkey kidney-derived Vero E6 and human colon carcinoma-derived Caco-2 cells were provided by American Type Culture Collection (ATCC). Cells were grown in high-glucose Dulbecco's modified Eagle's medium (DMEM) (Euroclone, Milan, Italy) supplemented with 10% fetal bovine serum (FBS) (Euroclone, Milan, Italy) at 37°C in humidified incubators with 5% CO<sub>2</sub>. SARS-CoV-2 strain was isolated from nasopharyngeal specimen taken from a patient with laboratory confirmed COVID-19 and was propagated in Vero E6 cells. Viral titres were determined by 50% tissue culture infectious dose (TCID<sub>50</sub>) assays in Vero E6 (Spearman-Kärber method) by microscopic scoring. All experiments were performed by infecting Vero E6 and Caco-2 cells with SARS-CoV-2 strain at the Department of Molecular Medicine, University of Padua, under Biosafety Level 3 (BSL3) protocols, in compliance with laboratory containment procedures approved by the University of Padua.

### ***Cytotoxicity assay***

Cytotoxicity was evaluated by incubating 100 and 500  $\mu$ g of bLf - the concentrations used for *in vitro* experiments - in DMEM containing 10% of FBS for 72 h at 37°C with Vero E6 and Caco-2 cells in

96-well microtiter plates. Cell proliferation and viability were assessed by MTT assay (Merck, Italy). Tetrazolium salts used for quantifying viable cells were cleaved to form a formazan dye, which was evaluated by spectrophotometric absorbance at 600 nm.

### ***Infection assay***

For infection assay, Vero E6 cells were seeded in 24-well tissue culture plates at a concentration of  $1 \times 10^5$  cells/well for 24h at 37°C in humidified incubators with 5% CO<sub>2</sub>, while Caco-2 cells were seeded at a concentration of  $2 \times 10^5$  cells/well for 48h at 37°C in humidified incubators with 5% CO<sub>2</sub>. 100 µg of bLf for Vero E6 infection assay, while 100 and 500 µg of bLf were used for Caco-2 infection assay. In order to investigate the putative interaction of bLf with viral particles and/or host cells, the following different experimental approaches were performed. To evaluate if bLf can interfere with the viral infectivity rate by binding viral surface components, SARS-CoV-2 at multiplicity of infection (MOI) of 0.1 and 0.01 was pre-incubated with bLf for 1h at 37°C in humidified incubators with 5% CO<sub>2</sub>. The cells were then infected with these suspensions for 1h at 37°C in humidified incubators with 5% CO<sub>2</sub>. In order to evaluate if bLf interferes with the viral attachment to host cells, the cells were pre-incubated in culture medium without FBS with bLf for 1h at 37°C in humidified incubators with 5% CO<sub>2</sub>. The cells were then washed with phosphate buffered saline (PBS) and infected with SARS-CoV-2 at MOI of 0.1 and 0.01 for 1h at 37°C in humidified incubators with 5% CO<sub>2</sub>. To assess if bLf can interfere with both viral and host cell components, bLf was added together with SARS-CoV-2 at MOI of 0.1 and 0.01 to cell monolayer for 1h at 37°C in humidified incubators with 5% CO<sub>2</sub>. In addition, the pre-incubation of SARS-CoV-2 with bLf for 1h at 37°C was used to infect cell monolayer previously pre-treated with bLf for 1 h at 37°C.

Regarding Vero E6 cells, after each experimental approach, the cells were washed with PBS, overlaid with DMEM containing 0.75% of carboxymethylcellulose and 2% of FBS and incubated for 48h at 37°C in humidified incubators with 5% CO<sub>2</sub>. After 48h, the cells were washed, fixed with 5% of formaldehyde for 10 min at room temperature and stained with crystal violet at 1% for 5 min. The number of plaques was determined after extensive washing.

The other infection experiments were carried out with Caco-2 cells. Substantial cell death was not detected up to 7 days on Caco-2 cells after SARS-CoV-2 infection at MOI 0.1 (Chu et al., 2020) (Chu et al. 2020). In this respect, after each experimental procedure, the cell monolayers were replaced with DMEM with 2% of FBS and after 6, 24 and 48 h post infection (hpi) the supernatant samples were collected for RNA extraction and quantitative real-time reverse transcription (RT)-PCR analysis of viral particles. Briefly, we lysed 200 µl of viral supernatant in an equal volume of NUCLISENS easyMAG lysis buffer (Biomerieux, France). Detection of SARS-CoV-2 RNA was performed by an in-house real-time RT-PCR method, which was developed according the protocol and the primers

and probes designed by Corman et al. (Corman et al., 2020) that targeted the genes encoding envelope (E) (E\_Sarbeco\_F, E\_Sarbeco\_R and E\_Sarbeco\_P1) of SARS-CoV-2. Quantitative RT-PCR assays were performed in a final volume of 25  $\mu$ l, containing 5  $\mu$ l of purified nucleic acids, using One Step Real Time kit (Thermo Fisher Scientific) and run on ABI 7900HT Fast Sequence Detection Systems (Thermo Fisher Scientific). Cycle threshold (Ct) data from RT-PCR assays were collected for E genes. Genome equivalent copies per ml were inferred according to linear regression performed on calibration standard curves.

### ***Protein-protein docking methods***

The structure of the SARS-CoV-2 spike glycoprotein in prefusion conformation was extracted from a clustering procedure carried out as indicated in a previously published paper (Romeo et al., 2020). The three-dimensional structure of the diferric forms of bovine and human lactoferrin, refined at 2.8 Å and 2.2 resolution respectively, were downloaded from the PDB Database (PDB IDs: 1BFL, (Lang et al., 2011) and 1B0L, (Sun et al., 1999)). The protein-protein docking analysis between the modelled SARS-CoV-2 spike glycoprotein<sup>1</sup> and the lactoferrin structures was carried out using the Frodock docking algorithm (Ramírez-Aportela et al., 2016). Frodock's approach combines the projection of the interaction terms into 3D grid-based potentials and the binding energy upon complex formation, which is approximated as a correlation function composed of van der Waals, electrostatics and desolvation potential terms. The interaction-energy minima are identified through a fast and exhaustive rotational docking search combined with a simple translational scanning (Garzon et al., 2009). Both docking procedures were performed using Frodock's (<http://frodock.chaconlab.org/>) web-server.

### ***Molecular dynamics***

Topology and coordinate files of the input structures were generated using the tLeap module of the AmberTools 19 package (Salomon-Ferrer et al., 2013). The spike glycoprotein and lactoferrin were parametrized using the ff19SB force field (Tian et al., 2020), and were inserted into a rectangular box of TIP3P water molecules (Jorgensen et al., 1983), with a minimum distance of 12.0 Å from the box sides, and after neutralizing the solution with 0.15 mol/L of NaCl ions. To remove unfavourable interactions, all structures underwent four minimization cycles, each composed by 500 steps of steepest descent minimization followed by 1500 steps of conjugated gradient minimization. An initial restraint of 20.0 kcal  $\cdot$  mol<sup>-1</sup>  $\cdot$  Å<sup>-2</sup> was imposed on protein atoms and subsequently reduced and removed in the last minimization cycle. Systems were gradually heated from 0 to 300 K in a NVT ensemble over a period of 2.0 ns using the Langevin thermostat (Loncharich et al., 1992), imposing a starting restraint of 0.5 kcal  $\cdot$  mol<sup>-1</sup>  $\cdot$  Å<sup>-2</sup> on each atom, which was decreased every 500 ps in order



to slowly relax the system. The systems were simulated in an isobaric-isothermal (NPT) ensemble for 2.0 ns, imposing a pressure of 1.0 atm using the Langevin barostat (Aoki et al., 2004) and fixing the temperature at 300 K. Covalent bonds involving hydrogen atoms were constrained using the SHAKE algorithm (Ryckaert et al., 1977). A production run of 30 ns was performed for with a timestep of 2.0 fs, using the NAMD 2.13 MD package (Phillips et al., 2005). The PME method was used to calculate long-range interactions (Darden et al., 1993), while a cut-off of 9.0 Å was set for short-range interactions. System coordinates were saved every 1000 steps.

### ***Trajectory analysis***

Distance analysis was performed using the distance module of the GROMACS 2019 analysis tools (Abraham et al., 2015), while hydrogen bond persistence was evaluated using the hbonds module coupled to in-house written codes. The hydrophobic contacts were identified using the *contact\_map* and *contact\_frequency* routines of the mdtraj Python library (McGibbon et al., 2015). Generalized Born and surface area continuum solvation (MM/GBSA) analysis (Genheden and Ryde, 2015) were performed over the last 15 ns of the trajectories, using the MMPBSA.py.MPI program implemented in the AMBER16 software (Case et al., 2016) on 2 nodes of the ENEA HPC cluster CRESCO6 (Ponti et al., 2014). Pictures of the Spike-Lactoferrin and Spike RBD-ACE2 complexes were generated using the UCSF Chimera program (Pettersen et al., 2004).

### ***Statistical analysis***

Descriptive and inferential statistical analyses were performed. The Kolmogorov–Smirnov test was used to check the normal distribution of blood parameters.

Blood parameters obtained at T0 in COVID-19 group and control group were compared using t-test. Data were then analyzed with a significant two-tailed p-value  $\leq 0.05$ .

All parameters obtained at T0 and T2 in COVID-19 group were then compared using paired t-test. In addition, the mean change between T0 and T2 was also assessed using paired t-test. Normally distributed data were then analyzed with a significant p-value  $\leq 0.05$ .

For what concerns in vitro experiments, the number of plaque forming units (pfu)/ml of SARS-CoV-2 on Vero E6 cells and the number of SARS-CoV-2 RNA copies/ml on Caco-2 cells in each experimental approach was compared with the control ones (untreated SARS-CoV-2 and cells) at the same time point in order to assess the statistically significant differences by using unpaired student's *t* tests. Results are expressed as the mean values  $\pm$  standard deviation (SD) of three independent experiments. In each case, a *p* value  $\leq 0.05$  was considered statistically significant.

## **RESULTS**

## ***Demographic data***

A total of 32 patients with confirmed COVID-19 infection at the real-time reverse transcription polymerase chain reaction (rRT-PCR) were recruited in the COVID-19 patients' group to participate in the study protocol. 22 patients had mild-to moderate symptoms and 10 patients were asymptomatic. The mean age was  $54.6 \pm 16.9$  years old. 14 patients were males and 18 females. The most prevalent comorbidity was hypertension (28%) followed by cardiovascular diseases (15.6%) and dementia (12.5%). 32 healthy volunteers (mean age  $52.8 \pm 15.5$  years old.) with negative rRT-PCR for SARS-CoV2 RNA were recruited in the control group to be paired to the above COVID-19 group. Patients group and control group were homogeneous for age and comorbidities. Clinic and demographic data of both groups are summarized in Tab.1.

## ***Primary Endpoint***

Real-time reverse transcription polymerase chain reaction (rRT-PCR) revealed a negative conversion of SARS-COV-2 RNA of the naso-oropharyngeal swab in 10 patients (31.25%) at T1 and in all other patients at T2, with all patients showed a viral clearance at T2 (Fig.1)

## ***Secondary Endpoints***

At T0, 22 patients were symptomatic and 10 patients asymptomatic. The most frequent symptoms were fatigue (50%), followed by arthralgia (37.5%) and cough (28%). At T1, 5 patients previously symptomatic became asymptomatic, with a total of 17 asymptomatic and 15 symptomatic patients. At T2 other 6 patients, previously symptomatic at T1, became asymptomatic with a total of 23 asymptomatic patients and 9 symptomatic patients. In the latter group, the most frequent symptom was fatigue (21.9%). Clinical symptoms are summarized in Fig. 2 and Fig. S1(supplemental data).

The comparison between COVID-19 group and control group parameters at T0 showed a significant difference in platelet count (p-value < 0,0001), neutrophils count (p-value= 0,04), monocytes count (p-value = 0,006), D-Dimer (< 0,0001), aspartate aminotransferase (AST) (p-value=0.008), ferritin (p-value < 0,0001), adrenomedullin (p-value< 0,0001) and IL-6 (p-value < 0,0001) (Tab. S1A, supplemental data).

Regarding COVID-19 group blood parameters, IL-6 value showed a significant decrease between T2 and T0 ( $\Delta_{T2-T0} -2.52 \pm 1.46$ , p-value 0.05). Moreover, D-dimer showed a significant decrease between T2 and T0 ( $\Delta_{T2-T0} -392.56 \pm 142.71$ , p-value 0.01) and ferritin presented the same significant trend ( $\Delta_{T2-T0} -90.63 \pm 48.49$ , p-value 0.04) (Tab. S1B, supplemental data). Regarding the other values we did not achieve a statistical significance, however we noticed an improvement in the platelet count

(T0: 239.63 ±83.05; T2: 243.70±65.5;  $\Delta_{T2-T0}$  10.05±10.26) and a decrease of alanine transaminase (ALT) (T0: 29.36±22.7; T2: 23.52±12.34;  $\Delta_{T2-T0}$  -7.32±4.36) and AST (T0:24.36±9.80;T2:22.64±8.33; $\Delta_{T2-T0}$ -2.68±2.52). Adrenomedullin remained at the same level all over the analyzed period ( $\Delta_{T2-T0}$ -0.01±0.03). IL-10 levels increased between T0 (8.67±3.26) and T2 (11.42±6.05), without showing statistical significance ( $\Delta_{T2-T0}$  2.55±2.09). TNF-alfa decreased between T2 (25.97±21.74) and T0 (37.34 ±19.95) without showing statistical significance ( $\Delta_{T2-T0}$  -12.92±8.81).

Regarding safety assessment, 2 patients (6.2%) showed gastrointestinal complaints related to Lf assumption at T2. The patients did not suspend Lf administration and the adverse event resolved itself spontaneously.

### ***Lactoferrin displays antiviral properties in in vitro models***

Preliminary, the doses of 100 and 500 µg/ml of bLf in native form (7% iron saturated) were assayed to detect their putative cytotoxicity by measuring cell morphology, proliferation and viability of Vero E6 and Caco-2 cell monolayers after 72 h of incubation. Both 100 and 500 µg/ml of bLf do not exert any cytotoxic effect (data not shown).

Then, the efficacy of different concentrations of bLf in inhibiting SARS-CoV-2 infection was tested on Vero E6 and Caco-2 cells according to different experimental procedures: i) control: untreated SARS-CoV-2 and cells; ii) bLf pre-incubated with virus inoculum for 1 h at 37°C before cell infection; iii) cells pre-incubated with bLf for 1 h at 37°C before virus infection; iv) bLf added together with virus inoculum at the moment of infection step; v) virus and cells separately pre-incubated with bLf for 1 h at 37°C before infection.

The results obtained with Vero E6 cells are shown in Figure 3A (MOI 0.1) and 3B (MOI 0.01).

Regarding Vero E6 cells, an inhibition of SARS-CoV-2 replication of about 1 log for MOI 0.1 and about 2 log for MOI 0.01 on cell monolayers was observed when 100 µg/ml of bLf were pre-incubated for 1 h with virus before infection compared to untreated SARS-CoV-2 infection ( $p < 0.001$  and  $p < 0.001$ , respectively) (Figure 3A and 3B).

On the contrary, the data illustrated in Figure 3A and 3B, independently from the MOI used, indicate that bLf, at this concentration, does not block SARS-CoV-2 infection when it is pre-incubated with Vero E6 cells or when bLf is contemporary added to viral particles and cells at the moment of infection (Figure 3A, 3B). BLf is also ineffective when it is pre-incubated for 1 h at 37°C separately with virus and cells before infection (Figure 3A, 3B).

The efficacy of 100 and 500 µg/ml of bLf against SARS-CoV-2, assayed in Caco-2 cells, is showed in Figure 4 A and B (MOI 0.1) and C and D (MOI 0.01), respectively.

Regarding Caco-2 cells, at MOI 0.1, no significant differences were observed in all experimental conditions compared to the control ones when using bLf at 100 µg/ml (Figure 4A). At MOI 0.01, an inhibition of viral load in supernatants was observed at 24 hpi only when 100 µg/ml of bLf was pre-incubated with the viral inoculum and when the cells were pre-incubated with 100 µg/ml of bLf compared to the control one ( $p < 0.05$ ) (Figure 4B). At 48 hpi, an inhibition of viral load was observed only when the cells were pre-incubated with bLf ( $p < 0.05$ ) (Figure 4B).

When bLf was used at a concentration of 500 µg/ml, a decrease of viral load up to 48 hpi was observed when the viral inoculum was pre-incubated with bLf compared to the control group, independently from the MOI used ( $p < 0.05$ ) (Figure 4C, 4D). When the cells were pre-incubated with bLf, a decrease of viral load up to 24 hpi was observed compared to the control at MOI 0.1 ( $p < 0.001$  after 6 hpi and  $p < 0.05$  after 24hpi) (Figure 4C), while at MOI 0.01 the decrease of viral load remained statistically significant up to 48 hpi compared to the control group ( $p < 0.05$ ) (Figure 4D). When bLf was added together with SARS-CoV-2 inoculum during the adsorption step a decrease of viral load up to 24 hpi was observed compared to untreated SARS-CoV-2 infection, independently from the MOI used ( $p < 0.001$  after 6 hpi and  $p < 0.05$  after 24hpi for MOI 0.1;  $p < 0.05$  after 6 and 24 hpi for MOI 0.01) (Figure 4C, 4D). When the cells were pre-incubated with bLf and infected with SARS-CoV-2 previously pre-incubated with bLf, a decrease of viral load up to 24 hpi was observed for MOI 0.1 compared to untreated SARS-CoV-2 infection ( $p < 0.001$  after 6 hpi and  $p < 0.05$  after 24hpi for MOI 0.1) (Figure 4C), while at MOI 0.01 the decrease of viral load remains statistically significant up to 48 hpi compared to untreated SARS-CoV-2 infection ( $p < 0.05$ ) (Figure 4D).

### ***Computational results***

The molecular docking simulation suggests a potential interaction of the bovine lactoferrin structure with the spike glycoprotein CDT1 domain in the up conformation (Fig. 5A). The first three solutions obtained by Frodock clustering procedure account for more than 60% of the total generated complexes, which are almost completely superimposable to that shown in Fig. 5A. Starting from the first Frodock solution, we performed a 30 ns long classical MD simulation in order to verify the stability of the complex and check for the presence of persistent interactions between the two proteins. As shown in figure S2A (supplemental data), the distance between the centers of the mass of Spike and lactoferrin, calculated as a function of time, oscillates around the value of 4.5 nm, indicating a constant close contact between the two molecules. MM/GBSA analysis confirmed the high affinity of the lactoferrin for the Spike CDT1 domain (Table S2A, supplemental data), showing interaction energy of -28.02 kcal/mol. In particular, MM/GBSA results highlighted that the Van der Waals term mainly contribute to the binding energy (Table S2A, supplemental data).

A detailed analysis of the interaction network reveals the presence of 28 different interactions, which persist for more than 25% of the simulation time, in agreement with the high interaction energy calculated. In detail, we found 3 salt bridges, 5 hydrogen bonds and 20 residue pairs involved in hydrophobic contacts (Table S3 left side, supplemental data).

To check if some of the Spike residues targeted by the lactoferrin protein are involved in the binding with ACE2, we have compared the average structure extracted from the simulation with the ACE2/CDT1 domain complex structure (PDB ID: 6LZG, Wang et al., 2020, Fig. 6). Surprisingly, only two Spike residues (Gly502 and Tyr505) are shared between the complexes interfaces (Table S3 left side, supplemental data), as evaluated from the inspection of the superimposed structures and from the paper analysis (Wang et al., 2020). Despite this, lactoferrin holds the same position assumed by the ACE2 enzyme, i.e. above the up CDT1 domain.

We performed the same analysis over the evaluated human lactoferrin-Spike complex, obtaining a binding pose superimposable to that observed for the bovine protein (Fig. 5B). Besides the fact that using the human protein we can still observe a persistent and close contact between the two molecules (Fig. S2B, supplemental data), the analysis of the interaction network reveals the presence of a larger number of interactions (45), in agreement with an higher interaction energy revealed by the MM/GBSA approach (-48,25 kcal/mol, Table S3 right side, supplemental data). In detail, we found 12 salt bridges, 10 hydrogen bonds and 23 residue pairs involved in hydrophobic contacts (Table S2B, supplemental data), in agreement with the presence of a negative electrostatic contribution term (Table S2B, supplemental data). Comparing the average structure extracted from the simulation with the ACE2/CDT1 domain complex structure (PDB ID: 6LZG<sup>21</sup> (Fig. S3, supplemental data), we observed that also for the human lactoferrin only two residues (Thr500 and Tyr505) are shared between the complexes interfaces (Table S3 right side, supplemental data).

These results allow us to hypothesize that, in addition to the HSPGs binding (Lang et al., 2011), both bovine and human lactoferrin should be able to hinder the spike glycoprotein attachment to the ACE2 receptor, consequently blocking the virus from entering into the cells.

## DISCUSSION

The current treatment approaches to COVID-19 have so far proved to be inadequate, and a potent antiviral drug or effective vaccine are yet to be discovered and eagerly awaited. The immediate priority is to harness innate immunity in order to accelerate early antiviral immune responses. Understanding the pathophysiology of COVID-19 is crucial to recognize target treatments to fight the virus. Hence, in this study, we focused our attention on the anti-viral and immunomodulating activity of Lf as an effective therapeutic option against COVID-19.

This is the first study assessing the use of Lf in the management of COVID-19 infection through *in vivo*, *in vitro* and *in silico* evidences.

Several evidences based on COVID-19 clinical epidemiology indicate the role of Lf in protecting against the virus also *in vivo*. Indeed, it has been reported that the incidence of COVID-19 in children aged 0-10 was only 0.9% in the Chinese cases, and infants developed a less severe disease form (Hong et al., 2020). Consecutively, some authors postulated that breast feeding or extensive use of Lf containing infant formula in this population may have protected from contagion or worst disease evolution (Chang et al., 2020).

Accordingly, we evaluated Lf role also *in vivo*, through a clinical trial, documenting its efficacy in favoring the viral clearance and the gradual symptoms recovery in COVID-19 patients with mild-to-moderate disease and in COVID-19 asymptomatic patients.

We focused our research on asymptomatic and mild-to-moderate COVID-19 patients, considering them a transmission reservoir with possible evolution to the most severe disease form (Jiang et al., 2020). Li et al, analyzing the viral shedding dynamics in asymptomatic and mildly symptomatic patients infected with SARS-CoV-2, observed a long-term viral shedding, also in the convalescent phase of the disease, where specific antibody production to SARS-CoV-2 may not guarantee viral clearance after hospital discharge. In their study, the median duration of viral shedding appeared to be shorter in pre-symptomatic patients (11.5 days) than in asymptomatic (28 days) and mild symptomatic cases (31 days) (Li et al., 2020b). In our study, Lf induced an early viral clearance just after 15 days from the beginning of the treatment in 31% of patients, and after 30 days of treatment in the rest of our patients. This early viral clearance allowed a reduction of viral shedding among our population, ensuring a decrease in the risk of transmission and contagion.

Although there are currently rare satisfactory markers for predicting the worsening of the disease until the death of patients with COVID-19, some cytokines, including IL-6, IL-10 and TNF $\alpha$ , and D-Dimer levels have been described as biomarkers related to a high case fatality of SARS-CoV-2 infection (Aziz et al., 2020; Li et al., 2020a; Tang et al., 2020; Ulhaq and Soraya, 2020; Xu et al., 2020b). In our study, we identified suitable deranged blood parameters to use as treatment target markers. Indeed, we found a statistically significant difference between the COVID-19 group and the control group in several blood parameters, including IL-6, D-Dimer, ferritin and liver function parameters. Particularly, IL-6, D-Dimer and ferritin also showed a significant decrease after Lf treatment confirming them as the most suitable COVID-19 treatment target markers.

Particularly, IL-6 elevation is considered to be associated with higher disease severity; IL-6 inhibitors, such as tocilizumab, have been used to treat severe COVID-19 patients (Cortegiani et al., 2020; Maeda et al.). The ability of Lf to down-regulate pro-inflammatory cytokines, such as IL-6, has already been demonstrated both in *in vitro* (Cutone et al., 2017; Frioni et al., 2014) and *in vivo* (Cutone et al., 2019; Valenti et al., 2017) models, as well as in clinical trials (Lepanto et al., 2018; Paesano et al., 2014), however this is the first evidence of its ability in down-regulating IL-6 also during SARS-CoV2 infection and thus the first proof of its efficacy for the treatment of COVID-19.

We observed also a statistically significant decline in D-Dimer levels, crucial to define disease prognosis, leading to a reduction in SARS-CoV-2 complications related to coagulation derangement. Recently, it was shown that Lf can regulate the activation of plasminogen and control coagulation cascade with a remarkable antithrombotic activity (Zwirzitz et al., 2018). Especially this Lf property should be stressed considering that COVID-19 is a prothrombotic disease and that the severity of the coagulation parameters impairment is related to a poor prognosis. Indeed, COVID-19 may represent a peculiar clinicopathologic form of viral sepsis, showing a prominent prothrombotic feature instead of the haemorrhagic one observed in other viral diseases. Patients affected by severe COVID-19 pneumonia are at higher risk of imbalance of coagulation parameters and thus treated with low molecular weight heparin or unfractionated heparin at doses registered for prevention of venous thromboembolism (Marietta et al., 2020). However, currently only severe patients are treated; this means that treatment may begin too late.

Our clinical experience suggests a role of Lf in preventing the evolution of the disease, improving the prognosis through its action on coagulation cascade when used since the first phases of the disease. Lf can exert negative regulatory effects on cell migration via inhibition of plasminogen activation and through the regulation of fibrinolysis (Zwirzitz et al., 2018). In addition, we observed an increased platelet count after Lf treatment. Indeed, COVID-19 induces thrombocytopenia as SARS-CoV-2 seems to entrap megakaryocytes and block the release of platelets. Lf rebalanced platelet count, induces COVID-19 viral clearance (Thachil, 2020).

Ferritin, besides reflecting the status of iron stores in healthy individuals, represents also an acute-phase-protein up-regulated and elevated in both infectious and non-infectious inflammation. In COVID-19, it has been reported to be relevant for assessing disease severity and patients outcome (Bolondi et al., 2020; Kappert et al., 2020). Iron chelators, such as Lf, have been repeatedly proposed as a potential therapeutic target during infections (Dalamaga et al., 2020) and even in COVID-19, we assessed the reduction of ferritin levels during Lf administration, demonstrating its ability to chelate iron, which is pivotal for bacterial and viral replication, and at the basis of its

antibacterial and antiviral activity(Berlutti et al., 2011; Valenti and Antonini, 2005; Wakabayashi et al., 2014).

Liver function is known to be deranged in COVID-19 and a meta-analysis showed that 16% and 20% of patients with COVID-19 had ALT and AST levels higher than the normal range(Deng et al., 2020). Liver biochemistry abnormality in COVID-19 patients could be ascribed to several factors, such as direct hepatocyte injury by the virus, drug-induced liver injury, hypoxic-ischemic microcirculation disorder, and underlying liver diseases (Xu et al., 2020b). In our study, we observed that Lf therapy reduced transaminases levels, decreasing the risk of liver-injury among COVID-19 patients, which is a very frequent complication in SARS-CoV2 severe forms (Wang et al., 2020). Moreover, since several treatments used to treat COVID-19 severe patients, such as hydroxychloroquine, are linked to liver injuries(Kelly et al., 2020), it could be rational to use Lf together with other therapies, in order to increase viral clearance and reduce adverse events of other treatments.

Adrenomedullin is another possible biomarker for COVID-19 prognosis, as it plays a key role in reducing vascular (hyper) permeability and promoting endothelial stability and integrity following severe infection (Wilson et al., 2020). Indeed, recent studies have suggested that COVID-19 induced endothelial dysfunction and damage could be the explanation for the development of organ dysfunction and edema, resulting in impaired vascular blood flow, coagulation and leakage(Varga et al., 2020). Thus, the development of endotheliitis may be a prominent, yet partly under recognized, feature of COVID-19 induced severe disease. In our study, we evaluated adrenomedullin levels in COVID-19 patients after receiving Lf treatment, which remained constant between T2 and T0. We explained this result considering the disease severity of our population. Indeed, adrenomedullin seems to vary in most severe patients(Christ-Crain et al., 2006).

Regarding clinical symptoms recovery, we observed a reduction in all symptoms, with the exception of fatigue, which persisted in 21.9 % of patients. We explained this result considering patients age and concomitant comorbidities, which could create a bias to identify COVID-19 symptoms.

Concerning Lf safety, we reported gastrointestinal complaints in 2 patients as occasional findings that did not lead to treatment discontinuation. Therefore, we concluded that Lf is safe and well tolerated among our study population.

In our analysis, we used formulations containing Apolactoferrin embedded in liposomes for nasal/oral administration. Indeed, the Apolactoferrin form is best suited to obtain the maximum chelating effect. Nucleic digestion, in the nasal cavities, and proteases and lipases hydrolysis, at gastric and intestinal level, inactivate the protein at its first entry, cancelling or extremely reducing the activity. Lf is



unstable in water and is particularly sensitive to bacterial and human proteases (enzymes inactivating proteins). This results in protein denaturation, poor absorption and inactivation. The inclusion of Lf in preserving structures, such as liposomes, reduces gastric and intestinal denaturation while maintaining its integrity and therefore its biological functionality(Aramaki et al., 1993; Boland, 2016; Ibraheem et al., 2014; Illum, 2002; Kato et al., 1993; Liu et al., 2017; Meshulam and Lesmes, 2014; Zhang et al., 2019).

The in vitro antiviral activity of bLf against enveloped and naked DNA and RNA viruses has been widely demonstrated(Arnold et al., 2002; Berlutti et al., 2011; Di Biase et al., 2003; Lang et al., 2011; Marchetti et al., 1999; Ng et al., 2015; Nozaki et al., 2003; Pietrantonio et al., 2003; Puddu et al., 1998; van der Strate et al., 2001; Superti et al., 1997; Wakabayashi et al., 2014), while few papers have been published on its in vivo efficacy against viral infection(Chen et al., 2008; Egashira et al., 2007; Hirashima et al., 2004; Ishibashi et al., 2005; L et al., 2013; Lu et al., 1987; Moriuchi M, 2009; Okada et al., 2002; Shin et al., 2005; Tanaka et al., 1999; Ueno et al., 2006; Vitetta et al., 2013; Yen et al., 2011).

The ability of bLf to inhibit viral infection is generally attributed to its binding to cell surface molecules and/or viral particles. BLf is able to competitively bind to heparan sulfate proteoglycans (HSPGs), present on the host cell surface and identified as initial sites for enveloped viruses(Sapp and Bienkowska-Haba, 2009; Spear, 2004), thus hindering the viral adhesion and internalization(Chien et al., 2008; Lang et al., 2011; Marchetti et al., 2004). Moreover, bLf can also bind directly to surface proteins of virus particles as HIV V3 loop of the gp120 (Swart et al., 1996) and HCV E2 envelope proteins(Nozaki et al., 2003).

The results, presented here, by monitoring the effect of bLf on different experimental procedures indicate that the antiviral activity of bLf, pre-incubated with host cells, seems to vary according to MOI, different cell lines and bLf concentration. As matter of fact, the pre-incubation of Vero E6 monolayers with 100 µg/ml of bLf, before SARS-CoV-2 infection at MOI 0.1 and 0.01, were ineffective in inhibiting virus internalization (Figure 3), differently to that observed when 100 µg/ml of bLf were pre-incubated with Caco-2 cells and the infection was performed at MOI 0.01 (Figure 4B). This antiviral activity was observed until 48 hpi.

The pre-incubation of 100 µg/ml of bLf with SARS-CoV-2 showed a significant antiviral activity higher at 0.01 MOI compared to 0.1 MOI after infection of Vero E6 cells (Figure 3A, 3B), while a significant antiviral activity assayed on Caco-2 cell lines was observed only with MOI 0.01 at 24 hpi (Figure 4B). In the other two experimental conditions, bLf did not show any significant antiviral activity on both Vero E6 and Caco-2 cells.

The pre-incubation of 500 µg/ml of bLf with Caco-2 cells showed a decrease of viral load until 24 hpi at MOI 0.1 and up to 48 hpi at MOI 0.01. Furthermore, the pre-incubation of 500 µg/ml of bLf with SARS-CoV-2 showed a significant decrease of SARS-CoV-2 RNA copies at both MOI 0.1 and 0.01. This antiviral activity persisted from 6 to 48 hpi (Figure 4C, 4D). In the other two experimental conditions, bLf exerted a significant antiviral activity only at 6 and 24 hpi when the MOI corresponded to 0.1 (Figure 4C). At MOI 0.01, a decrease of viral load up to 24 hpi was observed when bLf was added together with SARS-CoV-2 inoculum during the adsorption step (Figure 4D), while a decrease of viral load until 48 hpi was observed when both the cell monolayer and SARS-CoV-2 were previously pre-incubated with bLf (Figure 4D).

Our experimental results indicate that bLf exerts its antiviral activity either by direct attachment to the viral particles or by obscuring their cellular receptors. Moreover, the results obtained through the molecular docking and molecular dynamics simulation approaches strongly support the hypothesis of a direct recognition between the bLf and the spike S glycoprotein. The affinity between their molecular surfaces, the large number of atomistic interactions detected and their persistence during the simulation suggest that this recognition is very likely to occur and that bLf may hinder the spike S attachment to the human ACE2 receptor, consequently blocking the virus from entering into the cells.

Taken together these results reveal that, even if the definitive mechanism of action still has to be explored, the antiviral properties of Lf are also extendable to SARS-CoV-2 virus.

One of the limitations of our study was the small sample size of the clinical trial. Further studies, both in vitro and in vivo are needed to better deepen Lf placement against COVID-19, both as a preventive, adjunctive or definitive treatment. Nevertheless, we achieved a statistical significance in the crucial blood parameters related to disease evolution and we still observed an improving trend in all other analyzed markers. Further studies on larger samples are needed to better evaluate the role Lf in treating SARS-Cov-2.

Considering the risk of COVID19 relapse (Prévost et al., 2020), we also suggest additional long-term studies to evaluate the maintenance of viral clearance with Lf continuous administration.

Finally, due to ethical reasons, we could not include placebo arms in our study and therefore we could not evaluate properly the different disease evolution in treated and not-treated patients. However, considering the reported natural disease course (Li et al., 2020b) we can state Lf induced an early RT-PCR negative conversion and a fast clinical symptoms recovery.

This study is part of the GEFACOV2.0 research program coordinated by the Tor Vergata University of Rome

## Acknowledgements

We thank Prof. Denis Mariano for English language editing.

We thank Technology To Care (TDC) and mainly Dr. Biagio Biancardi, Dr. Martina Biancardi, Dr. Luigi Biancardi, for their expertise. In addition, we thank Dr. Alessandra Nistri and Prof. Maria Grazia Marciani and Prof. Giuseppe Novelli.

We thank Dr. Giancarlo Mennella of Egamid for technical support.

The computing resources and the related technical support were provided by CRESCO/ENEAGRID High Performance Computing infrastructure. CRESCO/ENEAGRID High Performance Computing infrastructure is funded by ENEA, the Italian National Agency for New Technologies, Energy and Sustainable Economic Development and by Italian and European research programmes, see <http://www.cresco.enea.it/english> for information.

**Author Contributions:** Conceptualization, EC, PV, LB, MF, AM; Formal analysis, CC; Investigation, EC, TC, LR, MPC, FI, AR, CDV, EF, SL, MM, MC, MN, AT, II, LC, AM, SB, NM, SS, FR, PLB; Writing- original draft, CL, EC, LR, LB, PV, MF; Writing-review & editing, EC, LB, PV

**Declaration of Interests:** none

## FIGURE LEGENDS

**Tab.1** Demographic and clinic data

**Figure 1** SARS-COV-2 RNA rRT-PCR trend

**Figure 2** Clinical symptoms recovery trend

**Figure 3** Plaque forming units (pfu)/ml of SARS-CoV-2 observed in Vero E6 cells infected at multiplicity of infection (MOI) of 0.1 (**A**) and 0.01 (**B**) in the presence or absence of 100 µg/ml of bovine lactoferrin (bLf) according to the following experimental procedures: i) control: untreated SARS-CoV-2 and Vero E6 cells; ii) bLf pre-incubated with SARS-CoV-2 inoculum for 1h at 37°C before cell infection iii) cells pre-incubated with bLf for 1 h at 37°C before SARS-CoV-2 infection; iv) bLf added together with SARS-CoV-2 inoculum during the adsorption step; v) virus and cells

separately pre-incubated with bLf for 1 h at 37°C before infection. Data represent the mean values of three independent experiments. Error bars: standard error of the mean. Statistical significance is indicated as follows: \*\*:  $p < 0.001$ , \*\*\*:  $p < 0.0001$  (Unpaired student's *t* test).

**Figure 4.** RNA copies/ml of SARS-CoV-2 observed in supernatants of Caco-2 cells infected at multiplicity of infection (MOI) of 0.1 (A,C) and 0.01 (B,D) in the presence or absence of 100 µg/ml (A,B) and 500 µg/ml (C,D) of bovine lactoferrin (bLf) according to the following experimental procedures: i) control: untreated SARS-CoV-2 and Caco-2 cells; ii) bLf pre-incubated with SARS-CoV-2 inoculum for 1h at 37°C before cell infection iii) cells pre-incubated with bLf for 1 h at 37°C before SARS-CoV-2 infection; iv) bLf added together with SARS-CoV-2 inoculum during the adsorption step; v) virus and cells separately pre-incubated with bLf for 1 h at 37°C before infection. Viral supernatant samples were harvested at 6, 24 and 48 hours post infection (hpi). Viral loads were ascertained with quantitative RT-PCR. Data represent the mean values of three independent experiments. Error bars: standard error of the mean. Statistical significance is indicated as follows: \*:  $p < 0.05$ , \*\*:  $p < 0.001$  (Unpaired student's *t* test).

**Figure 5:** Spacefill representations of the best molecular complex obtained with Frodock between the bovine (A) and human (B) lactoferrin with the Spike glycoprotein. The red, blue and green colours represent the Spike glycoprotein chains, while the yellow depicts the lactoferrin molecules.

**Figure 6:** Comparison of the Frodock best complex and of the ACE2-Spike glycoprotein (PDB ID: 6LZG). The red, blue and green solid surfaces represent the three different chains composing the Spike glycoprotein. The black ribbons highlight the CTD1 domain in the up conformation. The magenta and yellow ribbons represent the ACE2 (A) and the bovine lactoferrin (B), respectively, surrounded by a transparent molecular surface representation, in order to point out the positions occupied in the space by the different structures.

**Tab. 1**

Demographic Data		COVID-19 group		CONTROL group	
		Mean +/- SD	N (%)	Mean +/- SD	N (%)
Age		54.56 +/- 16.86		52.83 +/- 15.5	
Sex	male		14 (44%)		13 (41%)
	female		18 (56%)		19 (59%)
Mild-to moderate patients			22 (68.7%)		
Asymptomatic patients			10 (31%)		
Comorbidities	Hypertension		9 (28.1%)		7 (21.9%)
	Dementia		4 (12.5%)		1 (3.1%)
	Cardiovascular diseases		5 (15.625%)		5 (15.625%)
	HCV infection		2 (6.3%)		0
	Anemia		2 (6.3%)		2 (6.3%)
	Encephalopathy		3 (9.4%)		0
	Adenomatous Polyposis Coli		2 (6.3%)		0

**Fig. 1**

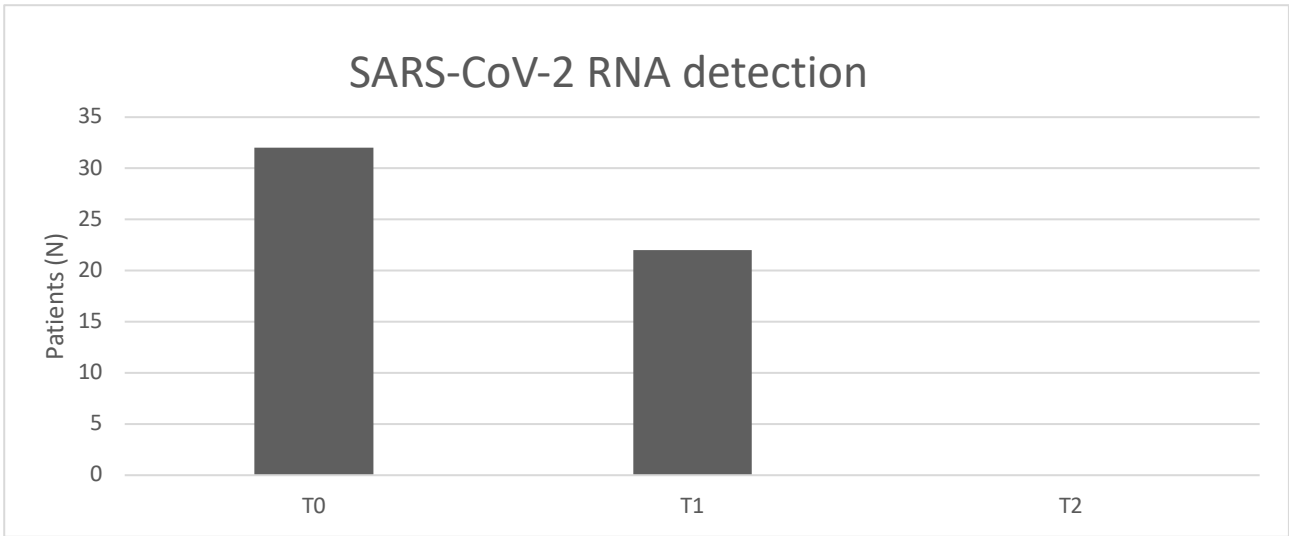


**Fig. 2**

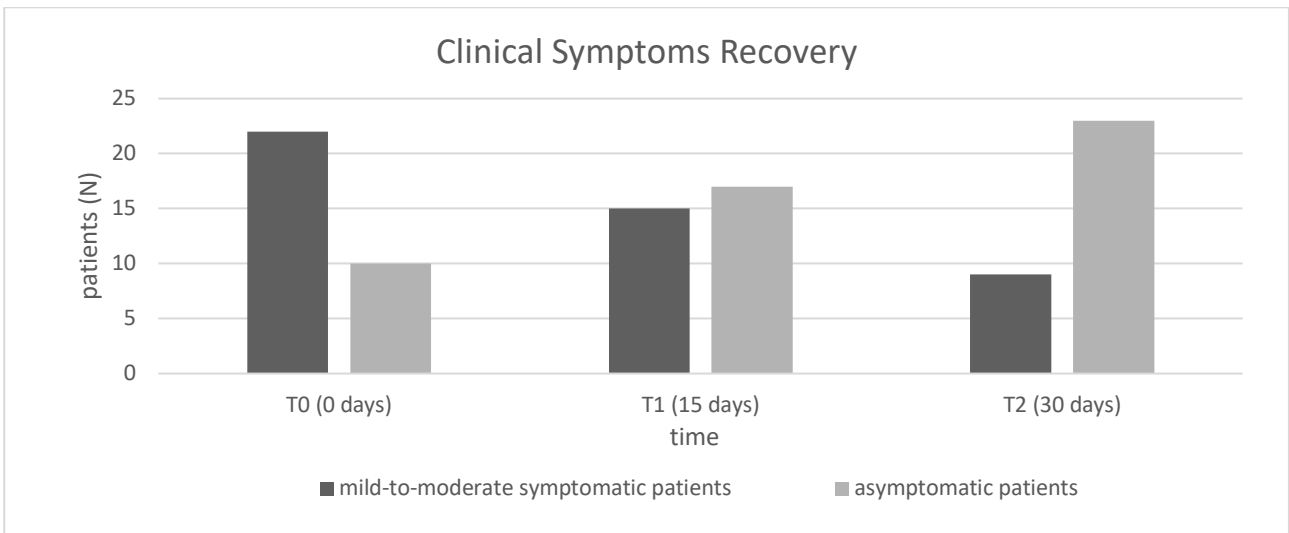


**Fig. 3**

**F**

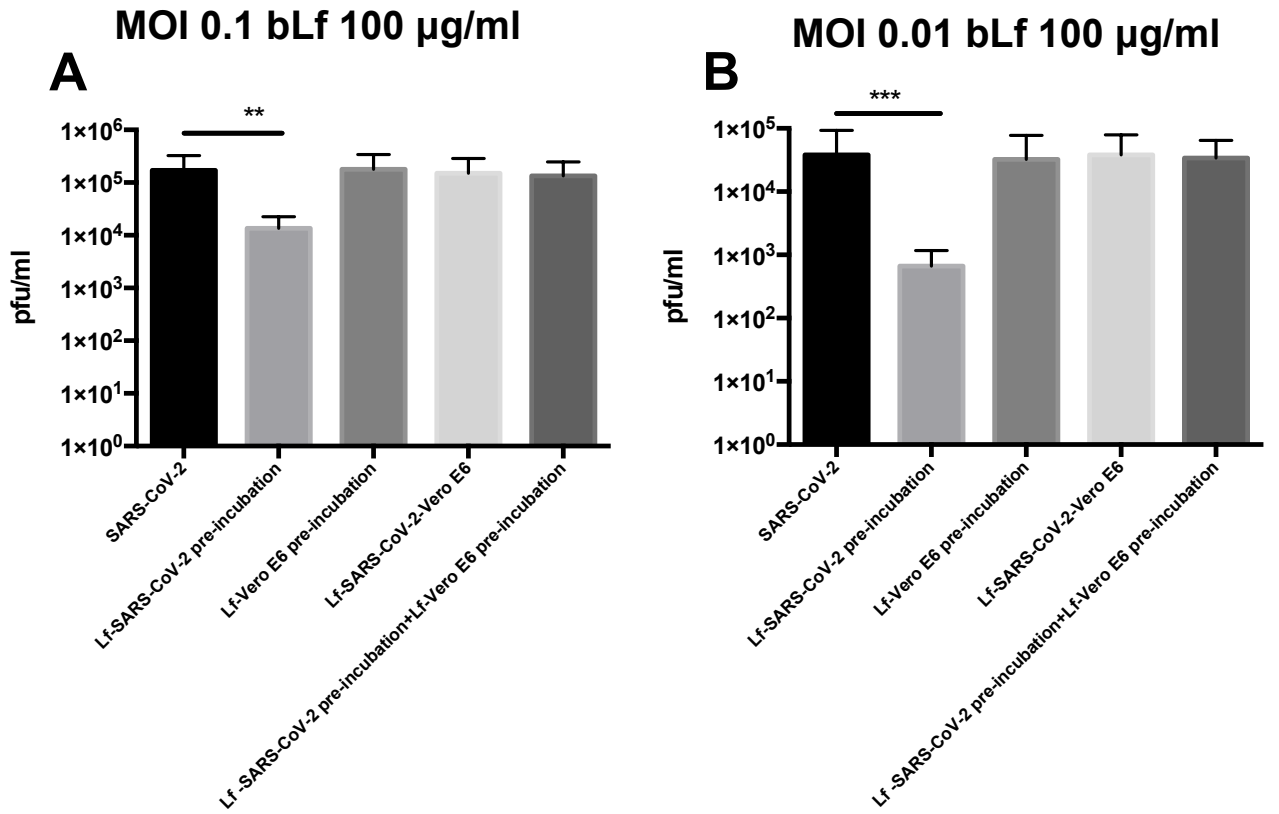
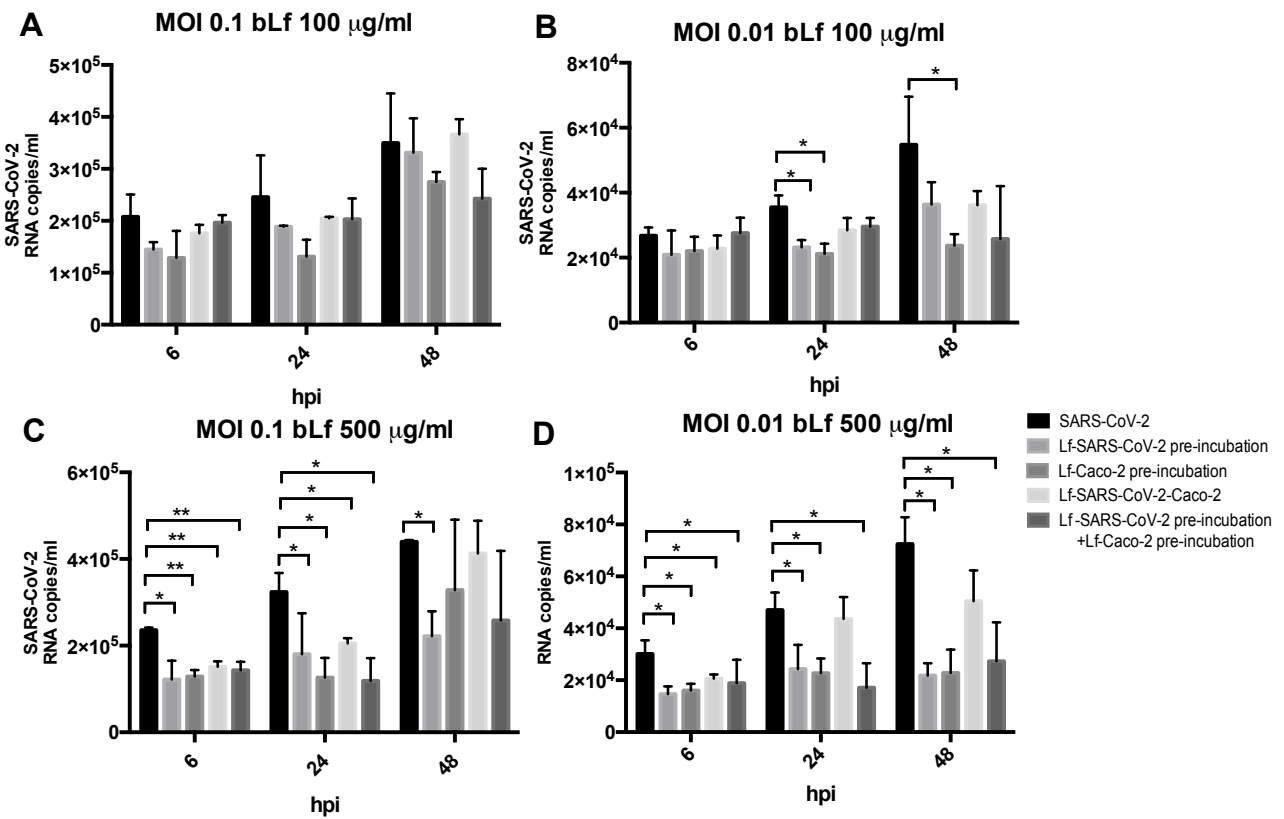
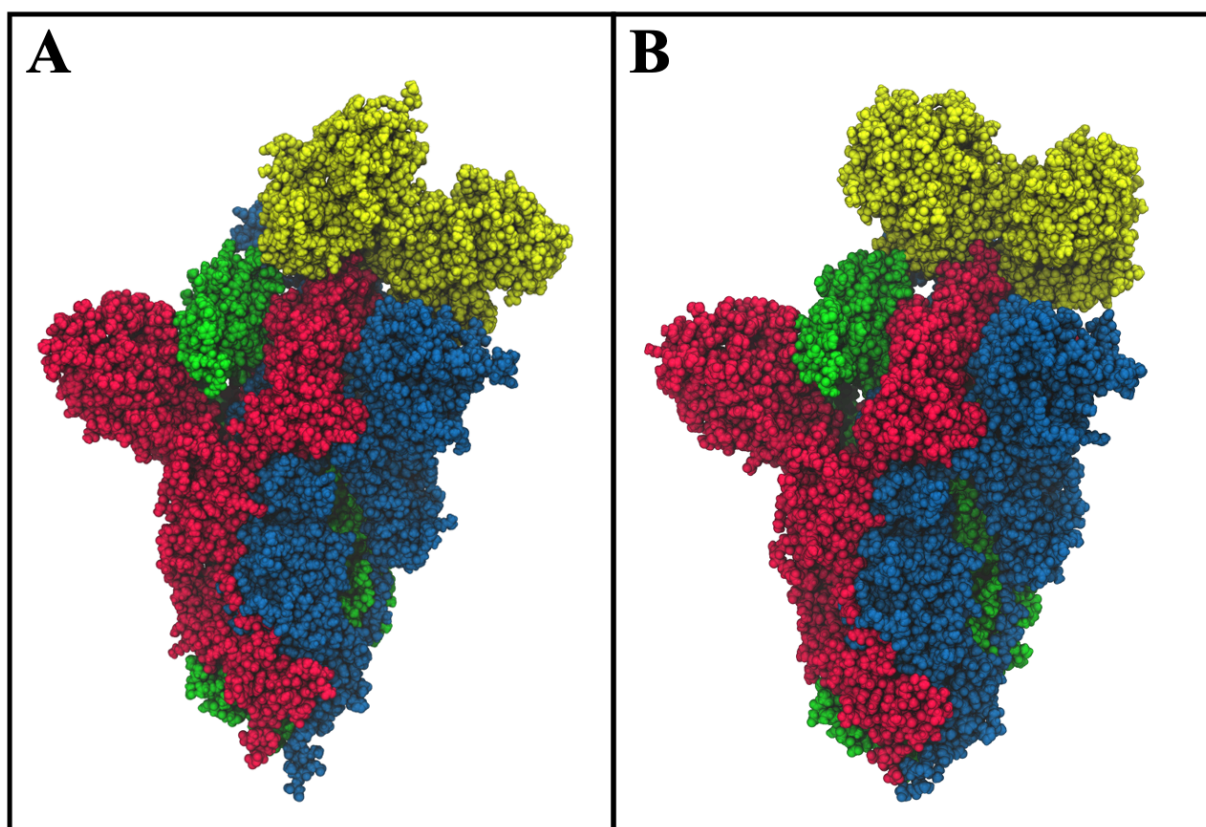


Fig. 4

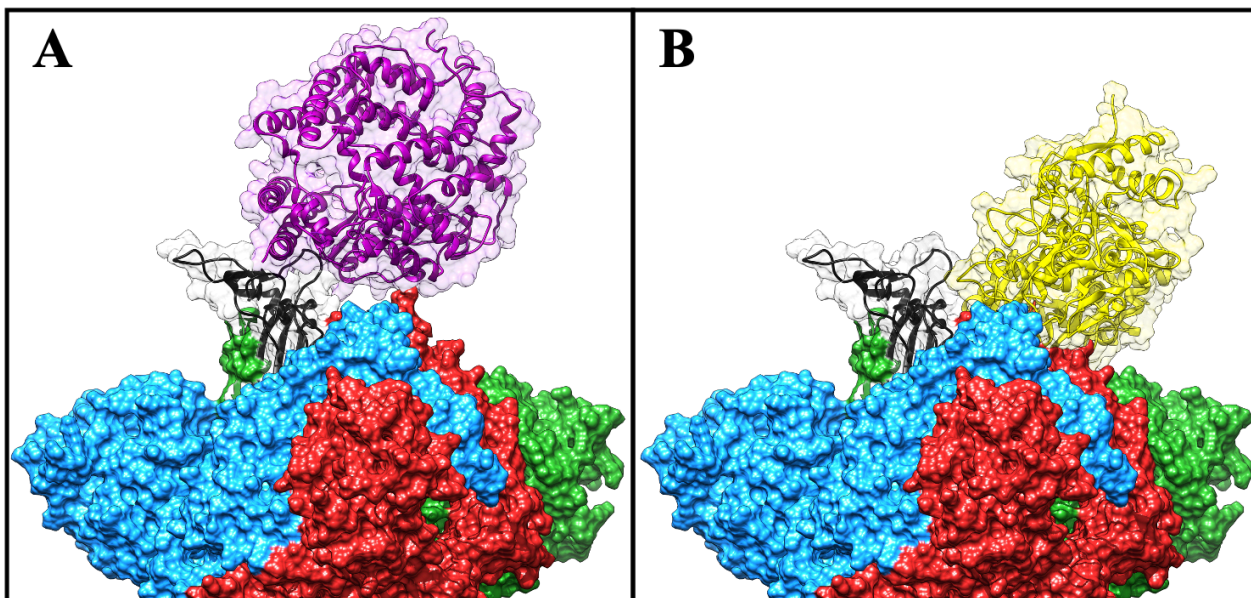




**Fig. 5**



**Fig. 6**



## REFERENCES

- Abraham, M.J., Murtola, T., Schulz, R., Páll, S., Smith, J.C., Hess, B., and Lindahl, E. (2015). GROMACS: High performance molecular simulations through multi-level parallelism from laptops to supercomputers. *SoftwareX* 1–2, 19–25.
- Aoki, K.M., Yoneya, M., and Yokoyama, H. (2004). Constant Pressure Md Simulation Method. *Molecular Crystals and Liquid Crystals* 413, 109–116.
- Aramaki, Y., Tomizawa, H., Hara, T., Yachi, K., Kikuchi, H., and Tsuchiya, S. (1993). Stability of liposomes in vitro and their uptake by rat Peyer's patches following oral administration. *Pharm. Res.* 10, 1228–1231.
- Arnold, D., Di Biase, A.M., Marchetti, M., Pietrantoni, A., Valenti, P., Seganti, L., and Superti, F. (2002). Antiadenovirus activity of milk proteins: lactoferrin prevents viral infection. *Antiviral Res.* 53, 153–158.
- Ashida, K., Sasaki, H., Suzuki, Y.A., and Lönnerdal, B. (2004). Cellular internalization of lactoferrin in intestinal epithelial cells. *Biometals* 17, 311–315.
- Aziz, M., Fatima, R., and Assaly, R. (2020). Elevated interleukin-6 and severe COVID-19: A meta-analysis. *J. Med. Virol.*
- Berlutti, F., Pantanella, F., Natalizi, T., Frioni, A., Paesano, R., Polimeni, A., and Valenti, P. (2011). Antiviral properties of lactoferrin--a natural immunity molecule. *Molecules* 16, 6992–7018.
- Boland, M. (2016). Human digestion--a processing perspective. *J. Sci. Food Agric.* 96, 2275–2283.
- Bolondi, G., Russo, E., Gamberini, E., Circelli, A., Meca, M.C.C., Brogi, E., Viola, L., Bissoni, L., Poletti, V., and Agnoletti, V. (2020). Iron metabolism and lymphocyte characterisation during Covid-19 infection in ICU patients: an observational cohort study. *World J Emerg Surg* 15.
- Campione, E., Cosio, T., Rosa, L., Lanna, C., Di Girolamo, S., Gaziano, R., Valenti, P., and Bianchi, L. (2020). Lactoferrin as Protective Natural Barrier of Respiratory and Intestinal Mucosa against Coronavirus Infection and Inflammation. *Int J Mol Sci* 21.
- Carsetti, R., Quintarelli, C., Quinti, I., Piano Mortari, E., Zumla, A., Ippolito, G., and Locatelli, F. (2020). The immune system of children: the key to understanding SARS-CoV-2 susceptibility? *Lancet Child Adolesc Health* 4, 414–416.

- Case, D., Betz, R., Cerutti, D., Cheatham, T., Darden, T., Duke, R., Giese, T., Gohlke, H., Goetz, A., and Homeyer, N. (2016). Amber 2016 (San Fr: Univ. California).
- Chang, R., Ng, T.B., and Sun, W.-Z. (2020). Lactoferrin as potential preventative and treatment for COVID-19. *Int. J. Antimicrob. Agents* 106118.
- Chang, R, Sun, WZ, and Ng, TB (2020). Lactoferrin as potential preventative and treatment for COVID-19. Authorea.
- Chen, H.-L., Wang, L.-C., Chang, C.-H., Yen, C.-C., Cheng, W.T.K., Wu, S.-C., Hung, C.-M., Kuo, M.-F., and Chen, C.-M. (2008). Recombinant porcine lactoferrin expressed in the milk of transgenic mice protects neonatal mice from a lethal challenge with enterovirus type 71. *Vaccine* 26, 891–898.
- Chien, Y.-J., Chen, W.-J., Hsu, W.-L., and Chiou, S.-S. (2008). Bovine lactoferrin inhibits Japanese encephalitis virus by binding to heparan sulfate and receptor for low density lipoprotein. *Virology* 379, 143–151.
- Christ-Crain, M., Morgenthaler, N.G., Stolz, D., Müller, C., Bingisser, R., Harbarth, S., Tamm, M., Struck, J., Bergmann, A., and Müller, B. (2006). Pro-adrenomedullin to predict severity and outcome in community-acquired pneumonia [ISRCTN04176397]. *Crit Care* 10, R96.
- Chu, H., Chan, J.F.-W., Yuen, T.T.-T., Shuai, H., Yuan, S., Wang, Y., Hu, B., Yip, C.C.-Y., Tsang, J.O.-L., Huang, X., et al. (2020). Comparative tropism, replication kinetics, and cell damage profiling of SARS-CoV-2 and SARS-CoV with implications for clinical manifestations, transmissibility, and laboratory studies of COVID-19: an observational study. *The Lancet Microbe* 1, e14–e23.
- Corman, V.M., Landt, O., Kaiser, M., Molenkamp, R., Meijer, A., Chu, D.K., Bleicker, T., Brünink, S., Schneider, J., Schmidt, M.L., et al. (2020). Detection of 2019 novel coronavirus (2019-nCoV) by real-time RT-PCR. *Euro Surveill.* 25.
- Cortegiani, A., Ippolito, M., Greco, M., Granone, V., Protti, A., Gregoret, C., Giarratano, A., Einav, S., and Cecconi, M. (2020). Rationale and evidence on the use of tocilizumab in COVID-19: a systematic review. *Pulmonology*.
- Cui, J., Li, F., and Shi, Z.-L. (2019). Origin and evolution of pathogenic coronaviruses. *Nat. Rev. Microbiol.* 17, 181–192.
- Cutone, A., Rosa, L., Lepanto, M.S., Scotti, M.J., Berlutti, F., Bonaccorsi di Patti, M.C., Musci, G., and Valenti, P. (2017). Lactoferrin Efficiently Counteracts the Inflammation-Induced Changes of the Iron Homeostasis System in Macrophages. *Front Immunol* 8, 705.
- Cutone, A., Lepanto, M.S., Rosa, L., Scotti, M.J., Rossi, A., Ranucci, S., De Fino, I., Bragonzi, A., Valenti, P., Musci, G., et al. (2019). Aerosolized Bovine Lactoferrin Counteracts Infection, Inflammation and Iron Dysbalance in A Cystic Fibrosis Mouse Model of Pseudomonas aeruginosa Chronic Lung Infection. *Int J Mol Sci* 20.
- Dalamaga, M., Karampela, I., and Mantzoros, C.S. (2020). Commentary: Could iron chelators prove to be useful as an adjunct to COVID-19 Treatment Regimens? *Metab. Clin. Exp.* 108, 154260.
- Darden, T., York, D., and Pedersen, L. (1993). Particle mesh Ewald: An N·log(N) method for Ewald sums in large systems. *J. Chem. Phys.* 98, 10089–10092.
- Deng, X., Liu, B., Li, J., Zhang, J., Zhao, Y., and Xu, K. (2020). Blood biochemical characteristics of patients with coronavirus disease 2019 (COVID-19): a systemic review and meta-analysis. *Clin. Chem. Lab. Med.* 58, 1172–1181.
- Di Biase, A.M., Pietrantonio, A., Tinari, A., Siciliano, R., Valenti, P., Antonini, G., Seganti, L., and Superti, F. (2003). Heparin-interacting sites of bovine lactoferrin are involved in anti-adenovirus activity. *J. Med.*

Viol. 69, 495–502.

Egashira, M., Takayanagi, T., Moriuchi, M., and Moriuchi, H. (2007). Does daily intake of bovine lactoferrin-containing products ameliorate rotaviral gastroenteritis? *Acta Paediatr.* 96, 1242–1244.

Forni, D., Cagliani, R., Clerici, M., and Sironi, M. (2017). Molecular Evolution of Human Coronavirus Genomes. *Trends Microbiol.* 25, 35–48.

Frioni, A., Conte, M.P., Cutone, A., Longhi, C., Musci, G., di Patti, M.C.B., Natalizi, T., Marazzato, M., Lepanto, M.S., Puddu, P., et al. (2014). Lactoferrin differently modulates the inflammatory response in epithelial models mimicking human inflammatory and infectious diseases. *Biometals* 27, 843–856.

Garzon, J.I., Lopéz-Blanco, J.R., Pons, C., Kovacs, J., Abagyan, R., Fernandez-Recio, J., and Chacon, P. (2009). FRODOCK: a new approach for fast rotational protein-protein docking. *Bioinformatics* 25, 2544–2551.

Genheden, S., and Ryde, U. (2015). The MM/PBSA and MM/GBSA methods to estimate ligand-binding affinities. *Expert Opin Drug Discov* 10, 449–461.

Gui, M., Song, W., Zhou, H., Xu, J., Chen, S., Xiang, Y., and Wang, X. (2017). Cryo-electron microscopy structures of the SARS-CoV spike glycoprotein reveal a prerequisite conformational state for receptor binding. *Cell Res.* 27, 119–129.

Hirashima, N., Orito, E., Ohba, K., Kondo, H., Sakamoto, T., Matsunaga, S., Kato, A., Nukaya, H., Sakakibara, K., Ohno, T., et al. (2004). A randomized controlled trial of consensus interferon with or without lactoferrin for chronic hepatitis C patients with genotype 1b and high viral load. *Hepatol. Res.* 29, 9–12.

Hong, H., Wang, Y., Chung, H.-T., and Chen, C.-J. (2020). Clinical characteristics of novel coronavirus disease 2019 (COVID-19) in newborns, infants and children. *Pediatr Neonatol* 61, 131–132.

Ibraheem, D., Elaissari, A., and Fessi, H. (2014). Administration strategies for proteins and peptides. *Int J Pharm* 477, 578–589.

Illum, L. (2002). Nasal drug delivery: new developments and strategies. *Drug Discov. Today* 7, 1184–1189.

Ishibashi, Y., Takeda, K., Tsukidate, N., Miyazaki, H., Ohira, K., Dosaka-Akita, H., and Nishimura, M. (2005). Randomized placebo-controlled trial of interferon alpha-2b plus ribavirin with and without lactoferrin for chronic hepatitis C. *Hepatol. Res.* 32, 218–223.

Jiang, X.-L., Zhang, X.-L., Zhao, X.-N., Li, C.-B., Lei, J., Kou, Z.-Q., Sun, W.-K., Hang, Y., Gao, F., Ji, S.-X., et al. (2020). Transmission Potential of Asymptomatic and Paucisymptomatic Severe Acute Respiratory Syndrome Coronavirus 2 Infections: A 3-Family Cluster Study in China. *J. Infect. Dis.* 221, 1948–1952.

Jorgensen, W.L., Chandrasekhar, J., Madura, J.D., Impey, R.W., and Klein, M.L. (1983). Comparison of simple potential functions for simulating liquid water. *J. Chem. Phys.* 79, 926–935.

Kappert, K., Jahić, A., and Tauber, R. (2020). Assessment of serum ferritin as a biomarker in COVID-19: bystander or participant? Insights by comparison with other infectious and non-infectious diseases. *Biomarkers* 0, 1–36.

Kato, Y., Hosokawa, T., Hayakawa, E., and Ito, K. (1993). Influence of liposomes on tryptic digestion of insulin. II. *Biol. Pharm. Bull.* 16, 740–744.

Kelly, M., O'Connor, R., Townsend, L., Coghlan, M., Relihan, E., Moriarty, M., Carr, B., Melanophy, G., Doyle, C., Bannan, C., et al. (2020). Clinical outcomes and adverse events in patients hospitalised with COVID-19, treated with off-label hydroxychloroquine and azithromycin. *Br J Clin Pharmacol.*

Kirchdoerfer, R.N., Wang, N., Pallesen, J., Wrapp, D., Turner, H.L., Cottrell, C.A., Corbett, K.S., Graham, B.S., McLellan, J.S., and Ward, A.B. (2018). Stabilized coronavirus spikes are resistant to conformational

changes induced by receptor recognition or proteolysis. *Sci Rep* 8, 15701.

Kruzel, M.L., Zimecki, M., and Actor, J.K. (2017). Lactoferrin in a Context of Inflammation-Induced Pathology. *Front Immunol* 8, 1438.

L, G., S, M., Am, G., O, R., A, W., and A, M. (2013). Lack of effect of bovine lactoferrin in respiratory syncytial virus replication and clinical disease severity in the mouse model (*Antiviral Res*).

Lan, J., Ge, J., Yu, J., Shan, S., Zhou, H., Fan, S., Zhang, Q., Shi, X., Wang, Q., Zhang, L., et al. (2020). Structure of the SARS-CoV-2 spike receptor-binding domain bound to the ACE2 receptor. *Nature* 581, 215–220.

Lang, J., Yang, N., Deng, J., Liu, K., Yang, P., Zhang, G., and Jiang, C. (2011). Inhibition of SARS pseudovirus cell entry by lactoferrin binding to heparan sulfate proteoglycans. *PLoS ONE* 6, e23710.

Lepanto, M.S., Rosa, L., Cutone, A., Conte, M.P., Paesano, R., and Valenti, P. (2018). Efficacy of Lactoferrin Oral Administration in the Treatment of Anemia and Anemia of Inflammation in Pregnant and Non-pregnant Women: An Interventional Study. *Front Immunol* 9, 2123.

Lepanto, M.S., Rosa, L., Paesano, R., Valenti, P., and Cutone, A. (2019). Lactoferrin in Aseptic and Septic Inflammation. *Molecules* 24.

Li, F. (2016). Structure, Function, and Evolution of Coronavirus Spike Proteins. *Annu Rev Virol* 3, 237–261.

Li, L.-Q., Huang, T., Wang, Y.-Q., Wang, Z.-P., Liang, Y., Huang, T.-B., Zhang, H.-Y., Sun, W., and Wang, Y. (2020a). COVID-19 patients' clinical characteristics, discharge rate, and fatality rate of meta-analysis. *J. Med. Virol.* 92, 577–583.

Li, W., Su, Y.-Y., Zhi, S.-S., Huang, J., Zhuang, C.-L., Bai, W.-Z., Wan, Y., Meng, X.-R., Zhang, L., Zhou, Y.-B., et al. (2020b). Viral shedding dynamics in asymptomatic and mildly symptomatic patients infected with SARS-CoV-2. *Clin. Microbiol. Infect.*

Liao, Y., Jiang, R., and Lönnnerdal, B. (2012). Biochemical and molecular impacts of lactoferrin on small intestinal growth and development during early life. *Biochem. Cell Biol.* 90, 476–484.

Liu, W., Wei, F., Ye, A., Tian, M., and Han, J. (2017). Kinetic stability and membrane structure of liposomes during in vitro infant intestinal digestion: Effect of cholesterol and lactoferrin. *Food Chem* 230, 6–13.

Loncharich, R.J., Brooks, B.R., and Pastor, R.W. (1992). Langevin dynamics of peptides: the frictional dependence of isomerization rates of N-acetylalanine-N'-methylamide. *Biopolymers* 32, 523–535.

Lu, L., Hangoc, G., Oliff, A., Chen, L.T., Shen, R.N., and Broxmeyer, H.E. (1987). Protective influence of lactoferrin on mice infected with the polycythemia-inducing strain of Friend virus complex. *Cancer Res.* 47, 4184–4188.

Lu, R., Zhao, X., Li, J., Niu, P., Yang, B., Wu, H., Wang, W., Song, H., Huang, B., Zhu, N., et al. (2020). Genomic characterisation and epidemiology of 2019 novel coronavirus: implications for virus origins and receptor binding. *Lancet* 395, 565–574.

Ludvigsson, J.F. (2020). Systematic review of COVID-19 in children shows milder cases and a better prognosis than adults. *Acta Paediatr.* 109, 1088–1095.

Maeda, T., Obata, R., Do, D.R., and Kuno, T. The Association of Interleukin-6 value, Interleukin inhibitors and Outcomes of Patients with COVID-19 in New York City. *Journal of Medical Virology* *n/a*.

Mancinelli, R., Rosa, L., Cutone, A., Lepanto, M.S., Franchitto, A., Onori, P., Gaudio, E., and Valenti, P. (2020). Viral Hepatitis and Iron Dysregulation: Molecular Pathways and the Role of Lactoferrin. *Molecules* 25.

- Marchetti, M., Superti, F., Ammendolia, M.G., Rossi, P., Valenti, P., and Seganti, L. (1999). Inhibition of poliovirus type 1 infection by iron-, manganese- and zinc-saturated lactoferrin. *Med. Microbiol. Immunol.* *187*, 199–204.
- Marchetti, M., Trybala, E., Superti, F., Johansson, M., and Bergström, T. (2004). Inhibition of herpes simplex virus infection by lactoferrin is dependent on interference with the virus binding to glycosaminoglycans. *Virology* *318*, 405–413.
- Marietta, M., Coluccio, V., and Luppi, M. (2020). COVID-19, coagulopathy and venous thromboembolism: more questions than answers. *Intern Emerg Med*.
- McGibbon, R.T., Beauchamp, K.A., Harrigan, M.P., Klein, C., Swails, J.M., Hernández, C.X., Schwantes, C.R., Wang, L.-P., Lane, T.J., and Pande, V.S. (2015). MDTraj: A Modern Open Library for the Analysis of Molecular Dynamics Trajectories. *Biophys. J.* *109*, 1528–1532.
- Menachery, V.D., Debbink, K., and Baric, R.S. (2014). Coronavirus non-structural protein 16: evasion, attenuation, and possible treatments. *Virus Res.* *194*, 191–199.
- Meshulam, D., and Lesmes, U. (2014). Responsiveness of emulsions stabilized by lactoferrin nano-particles to simulated intestinal conditions. *Food Funct* *5*, 65–73.
- Mirabelli, C., Wotring, J.W., Zhang, C.J., McCarty, S.M., Fursmidt, R., Frum, T., Kadambi, N.S., Amin, A.T., O'Meara, T.R., Pretto, C.D., et al. (2020). Morphological Cell Profiling of SARS-CoV-2 Infection Identifies Drug Repurposing Candidates for COVID-19. *BioRxiv*.
- Moriuchi M, M.H. (2009). Prevention of norovirus infection in nursery school children by intake of lactoferrin-containing products. 50th Japanese society of clinical virology,.
- Ng, T.B., Cheung, R.C.F., Wong, J.H., Wang, Y., Ip, D.T.M., Wan, D.C.C., and Xia, J. (2015). Antiviral activities of whey proteins. *Appl. Microbiol. Biotechnol.* *99*, 6997–7008.
- Nozaki, A., Ikeda, M., Naganuma, A., Nakamura, T., Inudoh, M., Tanaka, K., and Kato, N. (2003). Identification of a lactoferrin-derived peptide possessing binding activity to hepatitis C virus E2 envelope protein. *J. Biol. Chem.* *278*, 10162–10173.
- Okada, S., Tanaka, K., Sato, T., Ueno, H., Saito, S., Okusaka, T., Sato, K., Yamamoto, S., and Kakizoe, T. (2002). Dose-response trial of lactoferrin in patients with chronic hepatitis C. *Jpn. J. Cancer Res.* *93*, 1063–1069.
- Paesano, R., Pacifici, E., Benedetti, S., Berlutti, F., Frioni, A., Polimeni, A., and Valenti, P. (2014). Safety and efficacy of lactoferrin versus ferrous sulphate in curing iron deficiency and iron deficiency anaemia in hereditary thrombophilia pregnant women: an interventional study. *Biometals* *27*, 999–1006.
- Pettersen, E.F., Goddard, T.D., Huang, C.C., Couch, G.S., Greenblatt, D.M., Meng, E.C., and Ferrin, T.E. (2004). UCSF Chimera--a visualization system for exploratory research and analysis. *J Comput Chem* *25*, 1605–1612.
- Phillips, J.C., Braun, R., Wang, W., Gumbart, J., Tajkhorshid, E., Villa, E., Chipot, C., Skeel, R.D., Kalé, L., and Schulten, K. (2005). Scalable molecular dynamics with NAMD. *J Comput Chem* *26*, 1781–1802.
- Pietrantonio, A., Di Biase, A.M., Tinari, A., Marchetti, M., Valenti, P., Seganti, L., and Superti, F. (2003). Bovine lactoferrin inhibits adenovirus infection by interacting with viral structural polypeptides. *Antimicrob. Agents Chemother.* *47*, 2688–2691.
- Ponti, G., Palombi, F., Abate, D., Ambrosino, F., Aprea, G., Bastianelli, T., Beone, F., Bertini, R., Bracco, G., Caporicci, M., et al. (2014). The role of medium size facilities in the HPC ecosystem: the case of the new CRESCO4 cluster integrated in the ENEAGRID infrastructure. In 2014 International Conference on High Performance Computing Simulation (HPCS), pp. 1030–1033.

- Prévost, J., Gasser, R., Beaudoin-Bussi eres, G., Richard, J., Duerr, R., Laumaea, A., Anand, S.P., Goyette, G., Ding, S., Medjahed, H., et al. (2020). Cross-sectional evaluation of humoral responses against SARS-CoV-2 Spike. *BioRxiv*.
- Puddu, P., Borghi, P., Gessani, S., Valenti, P., Belardelli, F., and Seganti, L. (1998). Antiviral effect of bovine lactoferrin saturated with metal ions on early steps of human immunodeficiency virus type 1 infection. *Int. J. Biochem. Cell Biol.* *30*, 1055–1062.
- Ram rez-Aportela, E., L pez-Blanco, J.R., and Chac n, P. (2016). FRODOCK 2.0: fast protein-protein docking server. *Bioinformatics* *32*, 2386–2388.
- Romeo, A., Iacovelli, F., and Falconi, M. (2020). Targeting the SARS-CoV-2 spike glycoprotein prefusion conformation: virtual screening and molecular dynamics simulations applied to the identification of potential fusion inhibitors. *Virus Res* *286*, 198068–198068.
- Rosa, L., Cutone, A., Lepanto, M.S., Paesano, R., and Valenti, P. (2017). Lactoferrin: A Natural Glycoprotein Involved in Iron and Inflammatory Homeostasis. *Int J Mol Sci* *18*.
- Ryckaert, J.-P., Ciccotti, G., and Berendsen, H.J.C. (1977). Numerical integration of the cartesian equations of motion of a system with constraints: molecular dynamics of n-alkanes. *Journal of Computational Physics* *23*, 327–341.
- Salomon-Ferrer, R., Case, D.A., and Walker, R.C. (2013). An overview of the Amber biomolecular simulation package. *WIREs Computational Molecular Science* *3*, 198–210.
- Sapp, M., and Bienkowska-Haba, M. (2009). Viral entry mechanisms: human papillomavirus and a long journey from extracellular matrix to the nucleus. *FEBS J* *276*, 7206–7216.
- Shin, K., Wakabayashi, H., Yamauchi, K., Teraguchi, S., Tamura, Y., Kurokawa, M., and Shiraki, K. (2005). Effects of orally administered bovine lactoferrin and lactoperoxidase on influenza virus infection in mice. *J. Med. Microbiol.* *54*, 717–723.
- Spear, P.G. (2004). Herpes simplex virus: receptors and ligands for cell entry. *Cell. Microbiol.* *6*, 401–410.
- van der Strate, B.W., Beljaars, L., Molema, G., Harmsen, M.C., and Meijer, D.K. (2001). Antiviral activities of lactoferrin. *Antiviral Res.* *52*, 225–239.
- Su, S., Wong, G., Shi, W., Liu, J., Lai, A.C.K., Zhou, J., Liu, W., Bi, Y., and Gao, G.F. (2016). Epidemiology, Genetic Recombination, and Pathogenesis of Coronaviruses. *Trends Microbiol.* *24*, 490–502.
- Sun, X.-L., Baker, H.M., Shewry, S.C., Jameson, G.B., and Baker, E.N. (1999). Structure of recombinant human lactoferrin expressed in *Aspergillus awamori*. *Acta Crystallographica Section D* *55*, 403–407.
- Superti, F., Ammendolia, M.G., Valenti, P., and Seganti, L. (1997). Antirotaviral activity of milk proteins: lactoferrin prevents rotavirus infection in the enterocyte-like cell line HT-29. *Med. Microbiol. Immunol.* *186*, 83–91.
- Suzuki, Y.A., Wong, H., Ashida, K.-Y., Schryvers, A.B., and L nnerdal, B. (2008). The N1 domain of human lactoferrin is required for internalization by caco-2 cells and targeting to the nucleus. *Biochemistry* *47*, 10915–10920.
- Swart, P. j., Kuipers, M. e., Smit, C., Pauwels, R., De B thune, M. p., De Clercq, E., Meijer, D. k. f., and Huisman, J. g. (1996). Antiviral Effects of Milk Proteins: Acylation Results in Polyanionic Compounds with Potent Activity against Human Immunodeficiency Virus Types 1 and 2 in Vitro. *AIDS Research and Human Retroviruses* *12*, 769–775.
- Tanaka, K., Ikeda, M., Nozaki, A., Kato, N., Tsuda, H., Saito, S., and Sekihara, H. (1999). Lactoferrin inhibits hepatitis C virus viremia in patients with chronic hepatitis C: a pilot study. *Jpn. J. Cancer Res.* *90*, 367–371.

- Tang, N., Li, D., Wang, X., and Sun, Z. (2020). Abnormal coagulation parameters are associated with poor prognosis in patients with novel coronavirus pneumonia. *J. Thromb. Haemost.* *18*, 844–847.
- Thachil, J. (2020). What do monitoring platelet counts in COVID-19 teach us? *J. Thromb. Haemost.*
- Tian, X., Li, C., Huang, A., Xia, S., Lu, S., Shi, Z., Lu, L., Jiang, S., Yang, Z., Wu, Y., et al. (2020). Potent binding of 2019 novel coronavirus spike protein by a SARS coronavirus-specific human monoclonal antibody. *Emerg Microbes Infect* *9*, 382–385.
- Ueno, H., Sato, T., Yamamoto, S., Tanaka, K., Ohkawa, S., Takagi, H., Yokosuka, O., Furuse, J., Saito, H., Sawaki, A., et al. (2006). Randomized, double-blind, placebo-controlled trial of bovine lactoferrin in patients with chronic hepatitis C. *Cancer Sci.* *97*, 1105–1110.
- Ulhaq, Z.S., and Soraya, G.V. (2020). Interleukin-6 as a potential biomarker of COVID-19 progression. *Med Mal Infect* *50*, 382–383.
- Valenti, P., and Antonini, G. (2005). Lactoferrin: an important host defence against microbial and viral attack. *Cell. Mol. Life Sci.* *62*, 2576–2587.
- Valenti, P., Frioni, A., Rossi, A., Ranucci, S., De Fino, I., Cutone, A., Rosa, L., Bragonzi, A., and Berlutti, F. (2017). Aerosolized bovine lactoferrin reduces neutrophils and pro-inflammatory cytokines in mouse models of *Pseudomonas aeruginosa* lung infections. *Biochem. Cell Biol.* *95*, 41–47.
- Varga, Z., Flammer, A.J., Steiger, P., Haberecker, M., Andermatt, R., Zinkernagel, A.S., Mehra, M.R., Schuepbach, R.A., Ruschitzka, F., and Moch, H. (2020). Endothelial cell infection and endotheliitis in COVID-19. *Lancet* *395*, 1417–1418.
- Vitetta, L., Coulson, S., Beck, S.L., Gramotnev, H., Du, S., and Lewis, S. (2013). The clinical efficacy of a bovine lactoferrin/whey protein Ig-rich fraction (Lf/IgF) for the common cold: a double blind randomized study. *Complement Ther Med* *21*, 164–171.
- Wakabayashi, H., Oda, H., Yamauchi, K., and Abe, F. (2014). Lactoferrin for prevention of common viral infections. *J. Infect. Chemother.* *20*, 666–671.
- Wang, Q., Zhao, H., Liu, L.-G., Wang, Y.-B., Zhang, T., Li, M.-H., Xu, Y.-L., Gao, G.-J., Xiong, H.-F., Fan, Y., et al. (2020). Pattern of liver injury in adult patients with COVID-19: a retrospective analysis of 105 patients. *Mil Med Res* *7*, 28.
- Wilson, D.C., Schefold, J.C., Baldirà, J., Spinetti, T., Saeed, K., and Elke, G. (2020). Adrenomedullin in COVID-19 induced endotheliitis. *Crit Care* *24*.
- Wrapp, D., Wang, N., Corbett, K.S., Goldsmith, J.A., Hsieh, C.-L., Abiona, O., Graham, B.S., and McLellan, J.S. (2020). Cryo-EM Structure of the 2019-nCoV Spike in the Prefusion Conformation. *BioRxiv*.
- Xu, Y.-H., Dong, J.-H., An, W.-M., Lv, X.-Y., Yin, X.-P., Zhang, J.-Z., Dong, L., Ma, X., Zhang, H.-J., and Gao, B.-L. (2020a). Clinical and computed tomographic imaging features of novel coronavirus pneumonia caused by SARS-CoV-2. *Journal of Infection* *80*, 394–400.
- Xu, Z., Shi, L., Wang, Y., Zhang, J., Huang, L., Zhang, C., Liu, S., Zhao, P., Liu, H., Zhu, L., et al. (2020b). Pathological findings of COVID-19 associated with acute respiratory distress syndrome. *Lancet Respir Med* *8*, 420–422.
- Yen, M.-H., Chiu, C.-H., Huang, Y.-C., and Lin, T.-Y. (2011). Effects of lactoferrin-containing formula in the prevention of enterovirus and rotavirus infection and impact on serum cytokine levels: a randomized trial. *Chang Gung Med J* *34*, 395–402.
- Yuan, Y., Cao, D., Zhang, Y., Ma, J., Qi, J., Wang, Q., Lu, G., Wu, Y., Yan, J., Shi, Y., et al. (2017). Cryo-EM structures of MERS-CoV and SARS-CoV spike glycoproteins reveal the dynamic receptor binding domains. *Nat Commun* *8*, 15092.



Zhang, Y., Pu, C., Tang, W., Wang, S., and Sun, Q. (2019). Gallic acid liposomes decorated with lactoferrin: Characterization, in vitro digestion and antibacterial activity. *Food Chem* 293, 315–322.

Zwirzitz, A., Reiter, M., Skrabana, R., Ohradanova-Repic, A., Majdic, O., Gutekova, M., Cehlar, O., Petrovčíková, E., Kutejova, E., Stanek, G., et al. (2018). Lactoferrin is a natural inhibitor of plasminogen activation. *J. Biol. Chem.* 293, 8600–8613.